Structure of transcribing RNA polymerase II-nucleosome complex

Lucas Farnung[1*], Seychelle M. Vos[1*], and Patrick Cramer[1]

[1]Max Planck Institute for Biophysical Chemistry, Department of Molecular Biology, Am Fassberg 11, 37077 Göttingen, Germany. *These authors contributed equally.

Transcription of eukaryotic protein-coding genes requires passage of RNA polymerase II (Pol II) through chromatin. Pol II passage is impaired by nucleosomes and requires elongation factors that help Pol II to efficiently overcome the nucleosomal barrier[1-4]. How the Pol II machinery transcribes through a nucleosome remains unclear because structural studies have been limited to Pol II elongation complexes formed on DNA templates lacking nucleosomes[5]. Here we report the cryo-electron microscopy (cryo-EM) structure of transcribing Pol II from the yeast *Saccharomyces cerevisiae* engaged with a downstream nucleosome core particle (NCP) at an overall resolution of 4.4 Å. Pol II and the NCP adopt a defined orientation that could not be predicted from modelling. Pol II contacts DNA of the incoming NCP on both sides of the nucleosomal dyad with its domains 'clamp head' and 'lobe'. Comparison of the Pol II-NCP structure to known structures of Pol II complexes reveals that the elongation factors TFIIS, DSIF, NELF, PAF1 complex, and SPT6 can all be accommodated in the presence of the oriented nucleosome. Further structural comparisons show that the chromatin remodelling enzyme Chd1, which is also required for efficient Pol II passage[6,7], could bind the oriented nucleosome with its motor domain. The DNA-binding region of Chd1 must however be released from DNA when Pol II approaches the nucleosome, and based on published data[8,9] this is predicted to stimulate Chd1 activity and to facilitate Pol II passage. Our results provide a starting point for a mechanistic analysis of chromatin transcription.

To investigate how RNA polymerase II (Pol II) passes through chromatin, we determined the structure of Pol II transcribing into a nucleosome core particle (NCP). We initially attempted to obtain structures of elongating Pol II located at different positions within the NCP by placing transcription bubbles at different NCP locations, but these efforts were unsuccessful. We therefore switched to a minimal system and reconstituted Pol II

elongation complexes on pre-assembled, extended NCPs with different lengths of extranucleosomal DNA. The extended NCP that enabled structure determination comprised 145 base pairs (bp) of DNA with the Widom 601 sequence, 15 bp of extranucleosomal DNA, a 9-nucleotide (nt) 3'-DNA overhang, and a 10 nt RNA transcript annealed to the DNA overhang (Extended Data Fig. 1a). Pol II can bind the terminal DNA-RNA hybrid duplex of the extended NCP, resulting in a Pol II-NCP complex.

To test whether the reconstituted Pol II-NCP complex could elongate RNA, we incubated it with nucleoside triphosphates and transcription factor (TF) IIS, which is known to support Pol II elongation on nucleosomal templates[4]. We indeed observed RNA elongation (Extended Data Fig. 1b), demonstrating that the reconstituted complex was functional. RNA elongation stopped at several positions, indicating pausing of Pol II, and was almost completely blocked after addition of ~35 nt (Extended Data Fig. 1b). The block to RNA extension likely corresponds to the known major pause site around superhelical location (SHL) -5 of the NCP[3]. When we repeated the RNA elongation assay without histones, we observed extension to the end of the template (not shown), demonstrating that the presence of the NCP impairs RNA extension in this minimal system.

To prepare a sample for cryo-electron microscopy (cryo-EM), we again incubated reconstituted Pol II-NCP complex with nucleoside triphosphates and subjected the resulting complexes to size exclusion chromatography. TFIIS was initially included but lost during complex purification (Extended Data Fig. 1c, d). The peak fraction was analysed by cryo-EM with the use of a Krios microscope (FEI) equipped with a K2 detector (Gatan) (Methods). Analysis of the obtained cryo-EM single particle data revealed a well-defined Pol II-NCP complex that could be refined to an overall resolution of 4.4 Å (Fig. 1, Extended Data Fig. 2a-f). The resulting reconstruction showed well-defined protein secondary structure within Pol II and the histone octamer of the NCP (Extended Data Fig. 3).

We next placed crystal structures of the Pol II elongation complex[10] (PDB code 3HOV) and an NCP containing Widom 601 DNA[11] (PDB code 3LZ0) into the cryo-EM

density. The structures were locally adjusted to fit the density, connecting DNA was modelled, and the stereochemistry was refined (Methods). Despite extensive sorting of the cryo-EM particle images, we did not observe additional states of the Pol II-NCP complex with Pol II transcribing into the NCP. It is likely these states are unstable and did not survive preparation of the cryo-EM grids.

The structure reveals Pol II in the active, post-translocated state, positioned in front of the downstream nucleosome (Fig. 1, Extended Data Fig. 3f). The orientation of the NCP with respect to Pol II is defined, and differs from the predicted orientation. To predict the Pol II-NCP orientation, we positioned structures of Pol II and the NCP on the designed nucleic acid scaffold assuming that the connecting DNA adopts the canonical B-form conformation. In this model, the nucleosomal disc is rotated by ~95° compared to the orientation observed in our experimental structure (Extended Data Fig. 4). Comparison of the model with our structure also reveals that half a turn of nucleosomal DNA has been detached from the histone octamer surface. In particular, DNA base pairs between SHL -7 and SHL -6.5 are lifted from the octamer by up to 5 Å, and this enables feeding of the DNA into the polymerase active site cleft.

These observations indicate that the observed, distinct orientation of the NCP results from Pol II-NCP contacts. Indeed, the structure reveals two major contacts between Pol II and the nucleosome. Two Pol II domains that flank the polymerase cleft contact the NCP around its dyad axis (Fig. 2, Extended Data Fig. 2e, f). The clamp head domain in Pol II subunit Rpb1 contacts nucleosomal DNA at SHL +0.7, whereas the lobe domain of Rpb2 contacts SHL -0.7. Pol II-NCP contacts involve the protruding loops β4-β5 (Rpb1 residues 187-194) and α8-α9 (Rpb2 residues 333-345) in the clamp head and lobe, respectively (Fig. 2).

When Pol II encounters the first nucleosome in the transcribed region of a gene ('+1 nucleosome') it often pauses. In the fruit fly *D. melanogaster*, the +1 nucleosome is observed at a defined location 135-145 bps downstream of the transcription start site[12-14]. This positions the upstream edge of the +1 nucleosome at known sites for Pol II promoter-proximal pausing[14,15]. Superposition of the Pol II-NCP structure onto our recent paused elongation complex (PEC) structure[16] (PDB code 6GML) reveals that the oriented

NCP can be accommodated on the PEC without clashes with the pausing factors DSIF and NELF (Fig. 3a). In the resulting model, NELF subunit NELF-E and the C-terminal region of subunit NELF-B are located near the nucleosome. Whether and how pausing factors interact with the +1 nucleosome remains to be investigated.

Release of Pol II from pausing and passage of Pol II through nucleosomes requires several protein factors, including TFIIS, the PAF1 complex (PAF), and SPT6[4,17-21]. Superposition with our recent structure of the activated Pol II complex EC*[22] further shows that PAF and SPT6 can also be accommodated. In the resulting model, the C-terminus of the PAF subunit CTR9 is in close proximity to SHL +7 of nucleosomal DNA, explaining the known interaction of CTR9 with DNA[23] (Fig. 3b). The SPT6 N-terminal region is also located near the nucleosome, and is known to interact with the histone chaperone Spn1/IWS1[24,25], which could bind histones when Pol II progresses and unravels nucleosomal DNA.

Nucleosome passage also requires the ATP-dependent chromatin remodelling enzyme Chd1[6,7]. Comparison of the Pol II-NCP structure with our recent structure of the Chd1-NCP complex[26] after superposition of their NCPs revealed that the ATPase motor and the regulatory double chromodomain of Chd1 can be accommodated on the nucleosome surface without clashes with Pol II (Fig. 4). However, the DNA-binding region (DBR) of Chd1 would have to be displaced from its known position on extranucleosomal DNA[26,27] when transcribing Pol II approaches the NCP (Fig. 4). Previous studies showed that displacement of the DBR stimulates Chd1 ATPase activity[8,9]. Together these observations suggest that when Pol II approaches a Chd1-NCP complex, Pol II displaces the DBR of Chd1, thereby triggering full activation of the remodelling enzyme, which then loosens DNA-histone interactions. It however remains unclear how liberated histones could be transferred from downstream to upstream DNA, which involves the elongation factor FACT[1,28].

It was reported that Pol II passage can lead to transient displacement of one of the two H2A-H2B dimers, converting the histone octamer to a hexamer[29]. The observed Pol II-NCP contacts suggest that the observed orientation of the NCP remains the same during further Pol II transcription. In this scenario, the proximal H2A-H2B dimer would

encounter the clamp head and lobe domains when Pol II progresses by ~4-5 turns of DNA. The H2A-H2B dimer protrudes from the surface of the nucleosomal disc and would therefore clash with the clamp head, possibly leading to its displacement. It however remains enigmatic how downstream DNA can be propelled into the active site cleft when the nucleosomal disc does not rotate with respect to Pol II. It is possible that instead the histone octamer rotates in steps of one DNA turn around an axis normal to the nucleosomal disc to free DNA in ~10 bp portions, but this requires flexibility at the Pol II-NCP interface to accommodate minor changes in the length of DNA fed into the Pol II cleft.

In conclusion, the structure of a transcribing Pol II-NCP complex provides a starting point for analysis of the mechanisms of chromatin transcription. Over the next years, structures of Pol II-NCP complexes with relevant elongation factors such as TFIIS, PAF, SPT6, IWS1, CHD1 and FACT must be determined. Such structures hold the promise of revealing how elongation factors assist Pol II in nucleosome passage. Ultimately, these studies could provide the detailed mechanisms of chromatin transcription and reveal how the nucleosome is transferred from downstream to upstream DNA upon Pol II passage, to prevent loss of histones and the information of specific histone modifications during transcription.

We note that after our manuscript was essentially completed, others reported cryo-EM structures of Pol II-NCP complexes using a slightly different experimental strategy and complex reconstitution with nucleic acid scaffolds containing longer extranucleosomal DNA[30]. A detailed comparison of this very recent study with our work should allow for additional insights into Pol II passage through nucleosomes and facilitate future experiments.

Supplementary Information is available in the online version of the paper.

Acknowledgements We thank past and present members of the Cramer laboratory. We thank C. Burzinski for purification of *S. cerevisiae* Pol II and TFIIS. S.M.V. was supported by an EMBO Long-Term Fellowship (ALTF-725-2014). P.C. was supported by the Deutsche Forschungsgemeinschaft (SFB1064, SFB860), the European Research Council Advanced Investigator Grant TRANSREGULON (grant agreement No. 693023), and the Volkswagen Foundation.

Author Contributions L.F. carried out electron microscopy experiments and data processing. L.F. and S.M.V. carried out molecular biology, biochemistry and modelling work. P.C. designed and supervised research. L.F., S.M.V, and P.C. interpreted the data and wrote the manuscript.

Author Information The authors declare no competing financial interests. Readers are welcome to comment on the online version of the paper. Correspondence and requests for materials should be addressed to P.C. (pcramer@mpibpc.mpg.de).

Figure 1 | Structure of transcribing Pol II-NCP complex. a-c, Cartoon model viewed from the front (**a**), side (**b**), and top (**c**). Pol II subunits Rpb1, Rpb2, Rpb3, Rpb4, Rpb5, Rpb6, Rpb7, Rpb8, Rpb9, Rpb10, Rpb11, Rpb12, template DNA, non-template DNA, RNA, H2A, H2B, H3, and H4 are coloured in silver, sand, ruby, deep purple, slate, cyan, deepblue, forest green, orange, purple, yellow, green, blue, cyan, red, yellow, crimson, light blue, and green, respectively. Colour code used throughout. Histone octamer dyad axis is indicated as a black line with white outline.

Figure 2 | Pol II-NCP contacts. Rpb1 clamp head and Rpb2 lobe domains contact nucleosomal DNA around the NCP dyad. **a**, Side view. Clamp head and lobe domains are shown. Nucleosomal dyad axis, SHL -0.7 and +0.7 are indicated.

Figure 3 | Accommodation of elongation factors. Pol II complexes were superpositioned on the Pol II-NCP structure based on the Pol II core to model the location of elongation factors. **a**, Superposition with the mammalian paused elongation complex PEC (PDB code 6GML) locates DSIF and NELF. **b**, Superposition of the mammalian activated elongation complex EC* (PDB code 6GMH) locates PAF1 complex (PAF) and SPT6.

Figure 4 | Possible mechanism of Chd1 activation by Pol II. a, Superposition with the Chd1-NCP complex (PDB code 5O9G) by aligning the NCPs reveals that the DNA-binding region of Chd1 must be displaced from downstream DNA when Pol II approaches the NCP. Chd1 double chromodomain, ATPase lobe 1, ATPase lobe 2, and DNA-binding region are coloured in purple, orange, sea green, and pink, respectively.

METHODS

No statistical methods were used to predetermine sample size. The experiments were not randomized, and the investigators were not blinded to allocation during experiments and outcome assessment.

Protein preparation

S. cerevisiae Pol II was essentially purified as described[31]. *Xenopus laevis* histones were cloned, expressed, and purified as described[26,32,33]. *S. cerevisiae* TFIIS with an N-terminal GST tag was cloned, expressed, and purified as described[34].

Preparation of extended NCP

DNA fragments for nucleosome reconstitution were generated by PCR essentially as described[26,35]. A vector containing the Widom 601 sequence was used as a template for PCR. Large-scale PCR reactions were performed with two PCR primers (CGC TGT TTT CGA ATT TAC CCT TTA TGC GCC GGT ATT GAA CCA CGC TTA TGC CCA GCA TCG TTA ATC GAT GTA TAT ATC TGA CAC GTG CCT, reverse: ATC AGA ATC CCG GTG CCG AG) at a typical scale of 25 mL. The reaction was distributed into 48-well PCR plates (100 µl per well) and PCR was conducted with the following steps: 1. 98 °C for 1 min, 2. 98 °C for 10 s, 3. 72 °C for 45 s, cycle between steps 2 and 3 35 times, 4. 72 °C for 10 min, 5. Pause at 5 °C. PCR products were pooled, phenol chlorofom extracted, ethanol precipitated, and resuspended in 1 ml H_2O buffer. The sample was ethanol precipitated, resuspended in 500 µl H_2O buffer, and digested using TspRI (NEB) to generate the DNA 3'-overhang for RNA binding. Again, the digested DNA was phenol chlorofom extracted, ethanol precipitated and resuspended in 1 ml H_2O buffer. The DNA was then applied to a ResourceQ 6 ml (GE Healthcare) and eluted with a gradient from 0–100% TE high salt buffer (10 mM Tris pH 8.0, 1 M NaCl, 1 mM EDTA pH 8.0) over a total volume of 60 mL at a flow rate of 2 mL/min. Peak fractions were analysed on a 1% (v/v) TAE agarose gel and fractions containing the DNA product were pooled, ethanol precipitated, resuspended in 100 µL H_2O and stored at –20 °C. Preparation of extended NCP was performed as described[26]. Quantification of the reconstituted nucleosome was achieved by measuring absorbance at 280 nm. Molar

extinction coefficients were determined for protein and nucleic acid components and were summed to yield a molar extinction coefficient for the reconstituted extended NCP.

Reconstitution of Pol II-NCP complex

A RNA with the sequence /56-FAM/UCU CAC UGG A was purchased from Integrated DNA Technologies, resuspended in water, and stored at -80ºC. To reconstitute the Pol II-NCP complex, Pol II, extended NCP and RNA were mixed at a molar ratio of 1:0.5:0.66 and incubated for 10 min at 30ºC. Compensation buffer was added after 10 min to a final buffer of 150 mM KCl, 3 mM $MgCl_2$, 20 mM Na·HEPES pH 7.5, 4% (v/v) glycerol, 1 mM DTT. For RNA extension, we added TFIIS (1:0.57, relative to Pol II) and NTPs (1 mM final concentration) and incubated for 30 min at 30 °C. The reaction was centrifuged (21,000*g*, 4 °C, 10 min), and applied to a Superose 6 Increase 3.2/300 column equilibrated in gel filtration buffer (100 mM NaCl, 3 mM $MgCl_2$, 20 mM Na·HEPES pH 7.5, 5% (v/v) glycerol, 1 mM DTT). Peak fractions were analysed by SDS-PAGE and cross-linked with 0.1% (v/v) glutaraldehyde and incubated for 10 min on ice. The cross-linking reaction was quenched for 10 min using a concentration of 2 mM lysine and 8 mM aspartate. The sample was transferred to a Slide-A-Lyzer MINI Dialysis Unit 20,000 MWCO (Thermo Scientific), and dialysed for 6 h against 600 ml dialysis buffer (100 mM NaCl, 2 mM $MgCl_2$, 20 mM Na·HEPES pH 7.4, 20 mM Tris·HCl pH 7.5, 1 mM DTT).

RNA elongation assays

All concentrations refer to the final concentrations used in 70 µL reactions. Pol II (150 nM) was mixed with linear DNA or extended NCP (75 nM) and RNA primer (100 nM) at 30ºC. Compensation buffer was then added to achieve final assay conditions of 150 mM KCl, 3 mM $MgCl_2$, 20 mM Na·HEPES pH 7.5, 4% (v/v) glycerol, 1 mM DTT. TFIIS (90 nM) was added immediately before addition of NTPs. NTPs were added at a final concentration of 1 mM. 10 µL aliquots were taken at 0, 1, 5, 10, 20, and 30 minutes after NTP addition and were quenched by mixing the sample with 10 µL of Stop Buffer (6.4 M urea, 1x TBE, 50 mM EDTA pH 8.0). Reactions were treated with 4 µg proteinase K for 30 minutes at 30ºC. The reactions were ethanol precipitated and resuspended in 5 µL of Stop Buffer and applied to a 7 M urea, 13.5% 19:1 Bis-acrylamide, 1x TBE sequencing

gel run at 50W for 35 minutes in 1x TBE. RNA Products were visualized using the 6-FAM label and a Typhoon 9500 FLA Imager (GE Healthcare Life Sciences).

Cryo-EM and image processing

The reconstituted and purified Pol II-NCP complex sample was applied to R2/2 gold grids (Quantifoil). The grids were glow-discharged for 100 s before sample application of 2 µl on each side of the grid. The sample was subsequently blotted for 8.5 s and vitrified by plunging into liquid ethane with a Vitrobot Mark IV (FEI Company) operated at 4 °C and 100% humidity. Cryo-EM data were acquired on a FEI Titan Krios transmission electron microscope (TEM) operated at 300 keV, equipped with a K2 summit direct detector (Gatan). Automated data acquisition was carried out using FEI EPU software at a nominal magnification of 130,000×. Image stacks of 40 frames were collected in counting mode over 9 s. The dose rate was 5.12 e^- per $Å^2$ per s for a total dose of 46 e^- $Å^{-2}$. A total of 9188 image stacks were collected.

Frames were stacked and subsequently processed. Micrographs were CTF and motion corrected using Warp [36]. Image processing was performed with RELION 3.0-beta 1 [37] , unless noted otherwise. Post-processing of refined models was performed with automatic *B*-factor determination in RELION. Particles were picked using the neural network BoxNet2 of Warp, yielding 1,041,545 particle positions. Particles were extracted with a box size of 320^2 pixel, and normalized. Particles were subdivided into three batches. Using a 30 Å low-pass filtered model from a previously published model (EMDB-3626), we performed iterative rounds of hierarchical 3D classification with image alignment (and activated fast subset option) as outlined in Extended Data Fig. 2c. The three particle image batches were subsequently merged, and subjected to another round of 3D classification with image alignment. The best classes were combined and subjected to a 3D refinement with a mask that encompasses the entire Pol II-NCP complex. The Pol II-NCP reconstruction was obtained from 49,703 particles with an overall resolution of 4.4 Å (gold-standard Fourier shell correlation 0.143 criterion) [38]. The final map was sharpened with a *B*-factor of –182 $Å^2$. Local resolution estimates were determined using the built-in RELION tool for local resolution estimation.

Model building

Crystal structures of the *S. cerevisiae* Pol II EC (PDB code 3HOV) [10], and *X. laevis* nucleosome with Widom 601 sequence[11] (PDB code 3LZ0), were placed into the density using UCSF Chimera[39]. Extranucleosomal DNA and nucleosomal DNA from SHL −7 to SHL −5 were built using COOT[40]. Secondary structure restraints were applied and the model was real-space refined against the post-processed EM map using PHENIX[41]. Figures were generated using PyMol[42] and UCSF Chimera[39].

Data availability statement

The electron density reconstruction and final model were deposited with the Electron Microscopy Data Base (accession code XXXX) and with the Protein Data Bank (accession code XXXX).

Extended Data Figure 1| Formation of Pol II-NCP complex.

a, Schematic of nucleic acid scaffold used for RNA elongation assays and complex reconstitution for cryo-EM analysis. **b**, RNA elongation assays performed with Pol II (150 nM), NCP or linear DNA (75 nM), TFIIS (90 nM) with a FAM labelled 10mer RNA primer. Reactions were quenched at various time points. **c**, Formation of the Pol II-NCP complex on a Superose 6 Increase 3.2/30 size exclusion chromatography column. Blue and red curve shows absorption at 280 nm and 260 nm milli absorption units, respectively. **d**, SDS–PAGE of peak fraction from gel filtration (c) used for cryo-EM grid preparation containing Pol II and histones. The identity of the bands was confirmed by mass spectrometry. All experiments were performed at least three times.

Extended Data Figure 2| Cryo-EM structure determination

a, Representative micrograph, low pass filtered to enhance contrast. **b**, 2D class averages show Pol II in close proximity to a nucleosome. **c**, Sorting and classification tree used to reconstruct the Pol II-NCP complex at 4.4 Å resolution. **d**, Angular distribution. Shading from blue to yellow indicates the number of particles at a given orientation. **e**, Estimation of the average resolution. The dark green line indicates the Fourier shell correlation between the half maps of the reconstruction. Resolution is given for the FSC 0.143. The FSC 0.5 criterion is indicated. **f**, Local resolution estimation. Shading from red to blue indicates the local resolution according to the colour gradient. Absolute values are given.

Extended Data Figure 3| Cryo-EM densities. a-c, Locally filtered final map with model in side (a), front (b), and top (c) views. **d**, NCP from locally filtered final map. **e**, Rpb1 funnel helices on the Pol II surface are well defined. **f**, DNA-RNA hybrid in the Pol II active site adopts a post-translocated conformation with a free site for the nucleoside triphosphate substrate.

Extended Data Figure 4 | Comparison of the Pol II-NCP structure with a predicted model of the complex. Downstream DNA of a Pol II elongation complex was modelled with a total length of 15 base pairs, followed by a mononucleosome (PDB code 3LZ0, shown in grey) based on our nucleic acid scaffold design. The experimental structure is coloured with the same colouring scheme used throughout the publication. Difference in rotational position of the NCP is indicated.

Extended Data Table 1 | Cryo-EM data collection, refinement and validation statistics

References

1. Belotserkovskaya, R. *et al.* FACT Facilitates Transcription-Dependent Nucleosome Alteration. *Science* **301,** 1090–1093 (2003).
2. Teves, S. S., Weber, C. M. & Henikoff, S. Transcribing through the nucleosome. *Trends Biochem Sci* **39,** 577–586 (2014).
3. Studitsky, V. M., Clark, D. J. & Felsenfeld, G. Overcoming a nucleosomal barrier to transcription. *Cell* **83,** 19–27 (1995).
4. Kim, J., Guermah, M. & Roeder, R. G. The human PAF1 complex acts in chromatin transcription elongation both independently and cooperatively with SII/TFIIS. *Cell* **140,** 491–503 (2010).
5. Martinez-Rucobo, F. W. & Cramer, P. Structural basis of transcription elongation. *Biochim. Biophys. Acta* **1829,** 9–19 (2013).
6. Kwak, H. & Lis, J. T. Control of transcriptional elongation. *Annu. Rev. Genet.* **47,** 483–508 (2013).
7. Hauk, G. & Bowman, G. D. Structural insights into regulation and action of SWI2/SNF2 ATPases. *Curr Opin Struct Biol* **21,** 719–727 (2011).
8. McKnight, J. N., Jenkins, K. R., Nodelman, I. M., Escobar, T. & Bowman, G. D. Extranucleosomal DNA binding directs nucleosome sliding by Chd1. *Mol Cell Biol* **31,** 4746–4759 (2011).
9. Nodelman, I. M. *et al.* Interdomain Communication of the Chd1 Chromatin Remodeler across the DNA Gyres of the Nucleosome. *Mol Cell* **65,** 447–459.e6 (2017).
10. Sydow, J. F. *et al.* Structural Basis of Transcription: Mismatch-Specific Fidelity Mechanisms and Paused RNA Polymerase II with Frayed RNA. *Mol Cell* **34,** 710–721 (2009).
11. Vasudevan, D., Chua, E. Y. D. & Davey, C. A. Crystal structures of nucleosome core particles containing the '601' strong positioning sequence. *J Mol Biol* **403,** 1–10 (2010).
12. Mavrich, T. N. *et al.* Nucleosome organization in the Drosophila genome. *Nature* **453,** 358–362 (2008).

13. Gilmour, D. S. & Lis, J. T. RNA polymerase II interacts with the promoter region of the noninduced hsp70 gene in Drosophila melanogaster cells. *Mol Cell Biol* **6,** 3984–3989 (1986).
14. Zeitlinger, J. *et al.* RNA polymerase stalling at developmental control genes in the Drosophila melanogaster embryo. *Nat Genet* **39,** 1512–1516 (2007).
15. Gilchrist, D. A. *et al.* Pausing of RNA Polymerase II Disrupts DNA-Specified Nucleosome Organization to Enable Precise Gene Regulation. *Cell* **143,** 540–551 (2010).
16. Vos, S. M., Farnung, L., Urlaub, H. & Cramer, P. Structure of paused transcription complex Pol II-DSIF-NELF. *Nature* **560,** 601–606 (2018).
17. Adelman, K. *et al.* Efficient Release from Promoter-Proximal Stall Sites Requires Transcript Cleavage Factor TFIIS. *Mol Cell* **17,** 103–112 (2005).
18. Ng, H. H., Robert, F., Young, R. A. & Struhl, K. Targeted Recruitment of Set1 Histone Methylase by Elongating Pol II Provides a Localized Mark and Memory of Recent Transcriptional Activity. *Mol Cell* **11,** 709–719 (2003).
19. Yoh, S. M., Cho, H., Pickle, L., Evans, R. M. & Jones, K. A. The Spt6 SH2 domain binds Ser2-P RNAPII to direct Iws1-dependent mRNA splicing and export. *Genes Dev* **21,** 160–174 (2007).
20. Yoh, S. M., Lucas, J. S. & Jones, K. A. The Iws1:Spt6:CTD complex controls cotranscriptional mRNA biosynthesis and HYPB/Setd2-mediated histone H3K36 methylation. *Genes Dev* **22,** 3422–3434 (2008).
21. Bortvin, A. & Winston, F. Evidence that Spt6p controls chromatin structure by a direct interaction with histones. *Science* **272,** 1473–1476 (1996).
22. Vos, S. M. *et al.* Structure of activated transcription complex Pol II-DSIF-PAF-SPT6. *Nature* **560,** 607–612 (2018).
23. Musso, M., Bianchi-Scarrà, G. & Van Dyke, M. W. The yeast CDP1 gene encodes a triple-helical DNA-binding protein. *Nucleic Acids Res* **28,** 4090–4096 (2000).
24. Yoh, S. M., Cho, H., Pickle, L., Evans, R. M. & Jones, K. A. The Spt6 SH2 domain binds Ser2-P RNAPII to direct Iws1-dependent mRNA splicing and export. *Genes Dev* **21,** 160–174 (2007).
25. Li, S. *et al.* The elongation factor Spn1 is a multi-functional chromatin binding protein. *Nucleic Acids Res* **190,** 351 (2017).
26. Farnung, L., Vos, S. M., Wigge, C. & Cramer, P. Nucleosome-Chd1 structure and implications for chromatin remodelling. *Nature* **550,** 539–542 (2017).
27. Sundaramoorthy, R. *et al.* Structure of the chromatin remodelling enzyme Chd1 bound to a ubiquitinylated nucleosome. *eLife* **7,** (2018).
28. Formosa, T. *et al.* Defects in SPT16 or POB3 (yFACT) in Saccharomyces cerevisiae Cause Dependence on the Hir/Hpc Pathway: Polymerase Passage May Degrade Chromatin Structure. *Genetics* **162,** 1557–1571 (2002).
29. Kireeva, M. L. *et al.* Nucleosome remodeling induced by RNA polymerase II: loss of the H2A/H2B dimer during transcription. *Mol Cell* **9,** 541–552 (2002).
30. Kujirai, T. *et al.* Structural basis of the nucleosome transition during RNA polymerase II passage. *Science* eaau9904 (2018). doi:10.1126/science.aau9904
31. Lehmann, E., Brueckner, F. & Cramer, P. Molecular basis of RNA-dependent RNA polymerase II activity. *Nature* **450,** 445–449 (2007).
32. Dyer, P. N. *et al.* Reconstitution of nucleosome core particles from recombinant histones and DNA. *Methods Enzymol* **375,** 23–44 (2004).
33. Luger, K., Rechsteiner, T. J. & Richmond, T. J. Expression and purification of recombinant histones and nucleosome reconstitution. *Methods Mol Biol* **119,** 1–16 (1999).
34. Xu, Y. *et al.* Architecture of the RNA polymerase II-Paf1C-TFIIS transcription elongation complex. *Nat Comms* **8,** 15741 (2017).
35. Maskell, D. P. *et al.* Structural basis for retroviral integration into nucleosomes. *Nature* **523,** 366–369 (2015).
36. Tegunov, D. & Cramer, P. Real-time cryo-EM data pre-processing with Warp. *Science* 338558 (2018). doi:10.1101/338558

37. Zivanov, J. *et al.* RELION-3: new tools for automated high-resolution cryo-EM structure determination. *biorxiv.org* (2018). doi:10.1101/421123
38. Rosenthal, P. B. & Henderson, R. Optimal determination of particle orientation, absolute hand, and contrast loss in single-particle electron cryomicroscopy. *J Mol Biol* **333,** 721–745 (2003).
39. Pettersen, E. F. *et al.* UCSF Chimera--a visualization system for exploratory research and analysis. *J Comput Chem* **25,** 1605–1612 (2004).
40. Emsley, P., Lohkamp, B., Scott, W. G. & Cowtan, K. Features and development of Coot. *Acta Crystallogr. D Biol. Crystallogr.* **66,** 486–501 (2010).
41. Adams, P. D. *et al.* PHENIX: a comprehensive Python-based system for macromolecular structure solution. *Acta Crystallogr. D Biol. Crystallogr.* **66,** 213–221 (2010).
42. PyMOL. The PyMOL Molecular Graphics System, Version 1.5.0.4 Schrödinger, LLC.

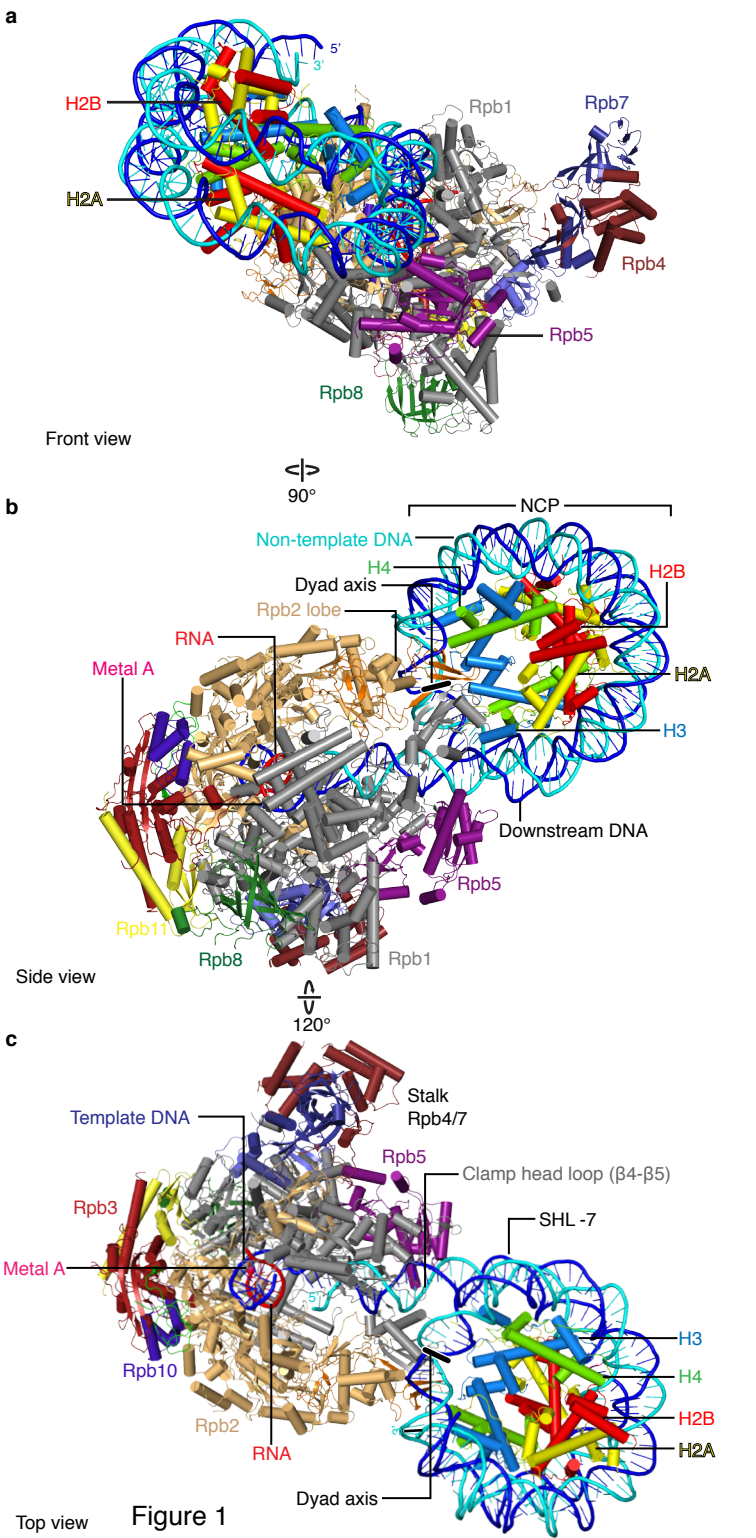
a
5'
3'
H2B
H2A
Rpb1
Rpb7
Rpb4
Rpb5
Rpb8
Front view
90°
b
NCP
Non-template DNA
H4
Dyad axis
H2B
Rpb2 lobe
RNA
Metal A
H2A
H3
Downstream DNA
Rpb5
Rpb11
Rpb8
Rpb1
Side view
120°
c
Stalk
Rpb4/7
Template DNA
Rpb5
Clamp head loop (β4-β5)
Rpb3
SHL -7
Metal A
5'
H3
Rpb10
H4
H2B
Rpb2
RNA
H2A
Dyad axis
Top view

Figure 1

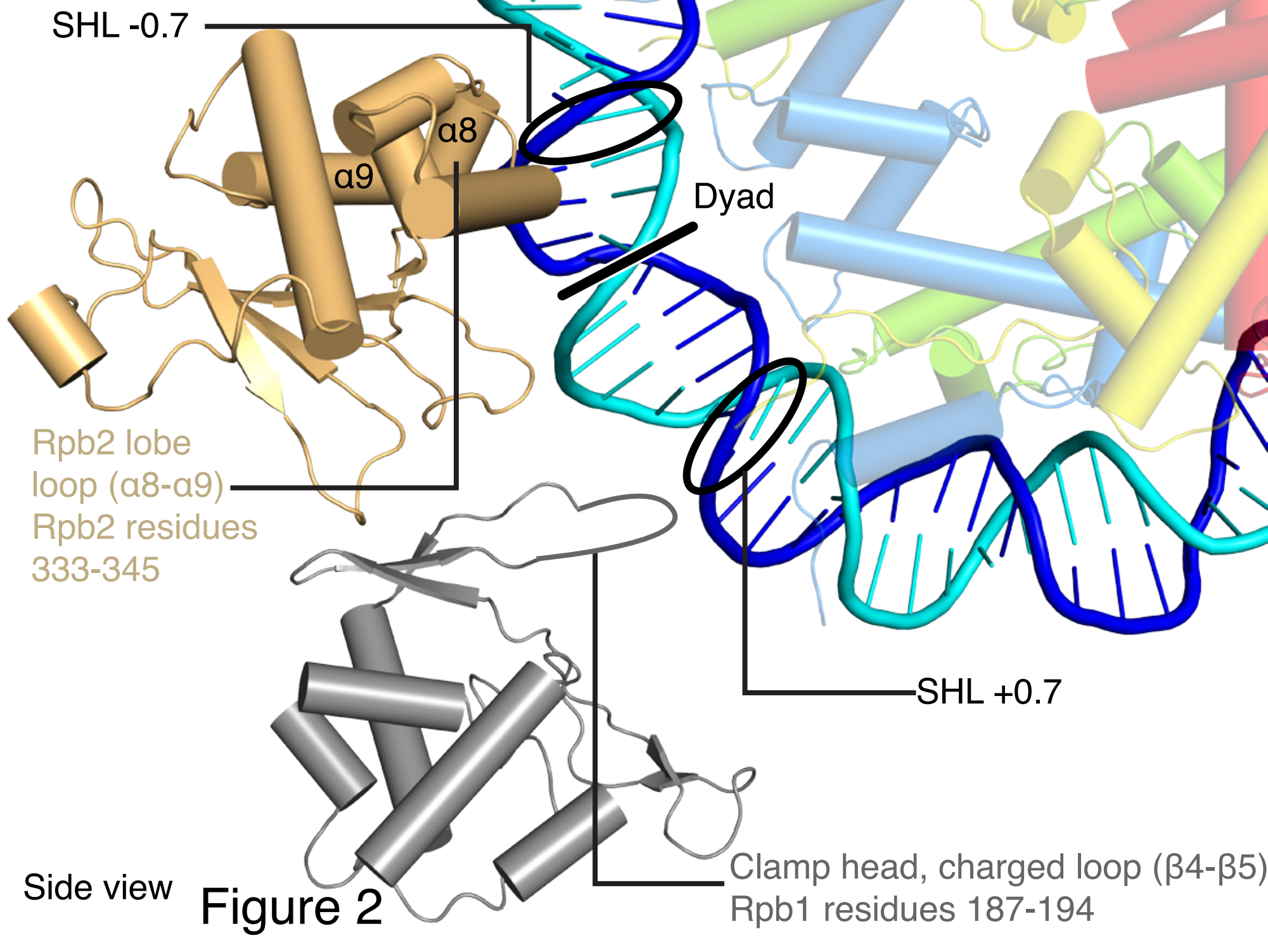
SHL -0.7
α8
α9
Dyad
Rpb2 lobe
loop (α8-α9)
Rpb2 residues
333-345
SHL +0.7
Clamp head, charged loop (β4-β5)
Rpb1 residues 187-194
Side view

Figure 2

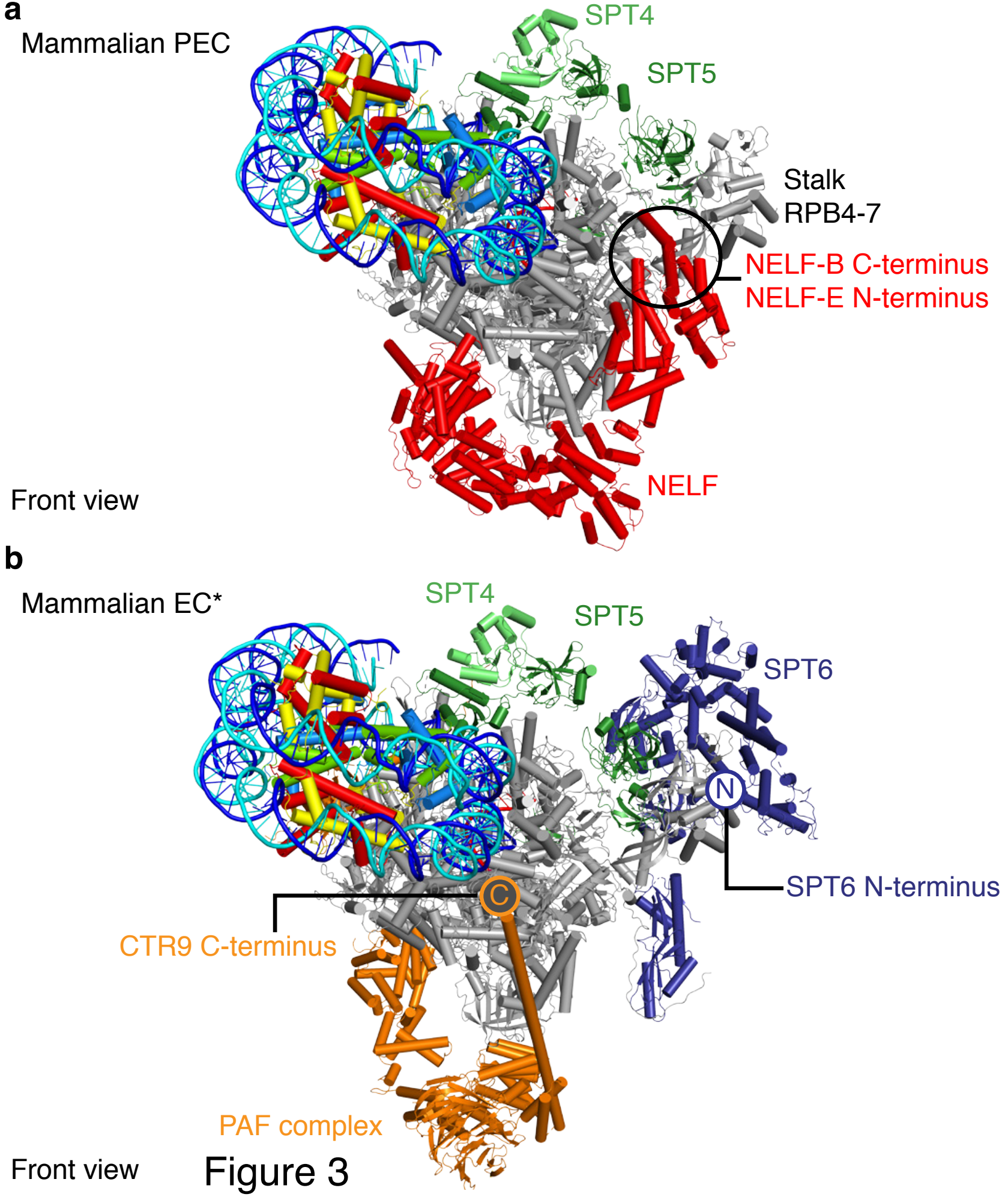
a
Mammalian PEC
SPT4
SPT5
Stalk
RPB4-7
NELF-B C-terminus
NELF-E N-terminus
NELF
Front view
b
Mammalian EC*
SPT4
SPT5
SPT6
N
SPT6 N-terminus
C
CTR9 C-terminus
PAF complex
Front view

Figure 3

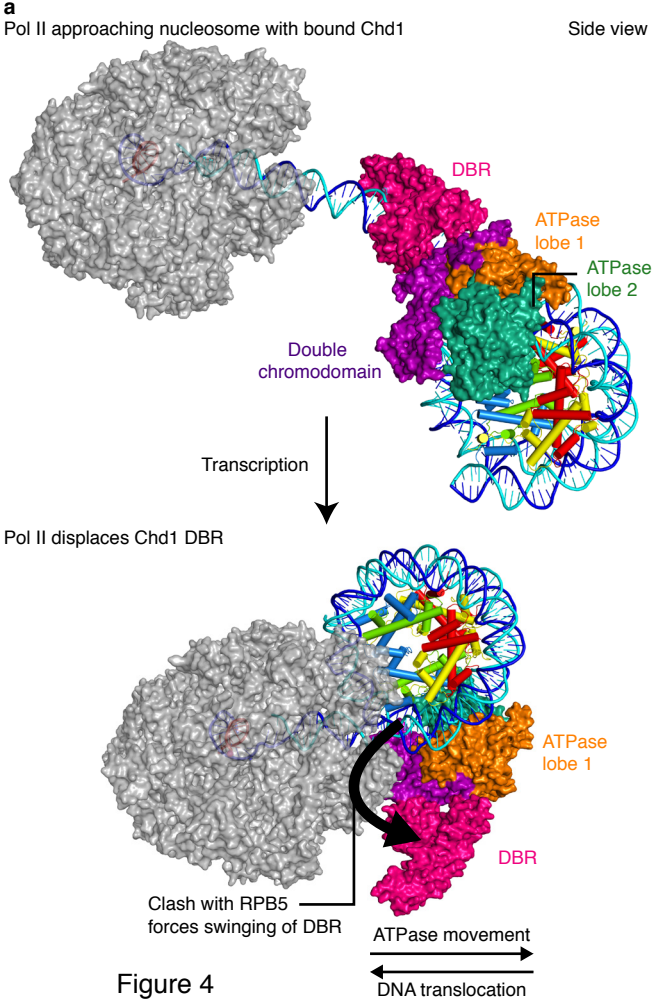
a
Pol II approaching nucleosome with bound Chd1
Side view
DBR
ATPase
lobe 1
ATPase
lobe 2
Double
chromodomain
Transcription
Pol II displaces Chd1 DBR
ATPase
lobe 1
DBR
Clash with RPB5
forces swinging of DBR
ATPase movement
DNA translocation

Figure 4

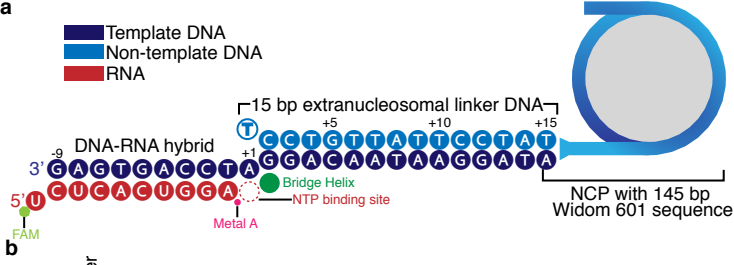

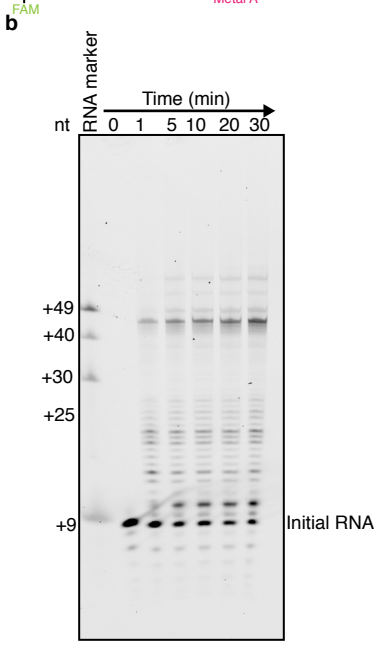

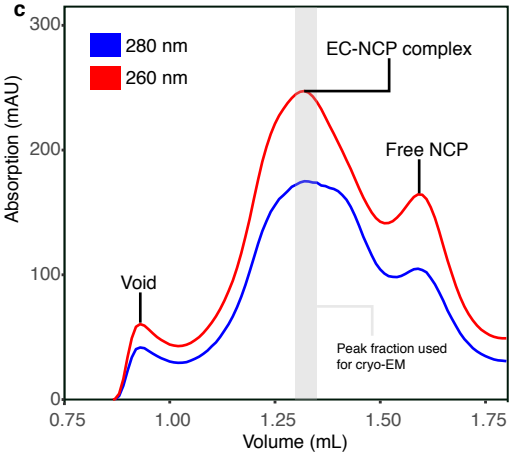

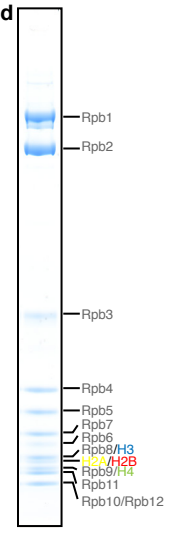

Extended Data Figure 1

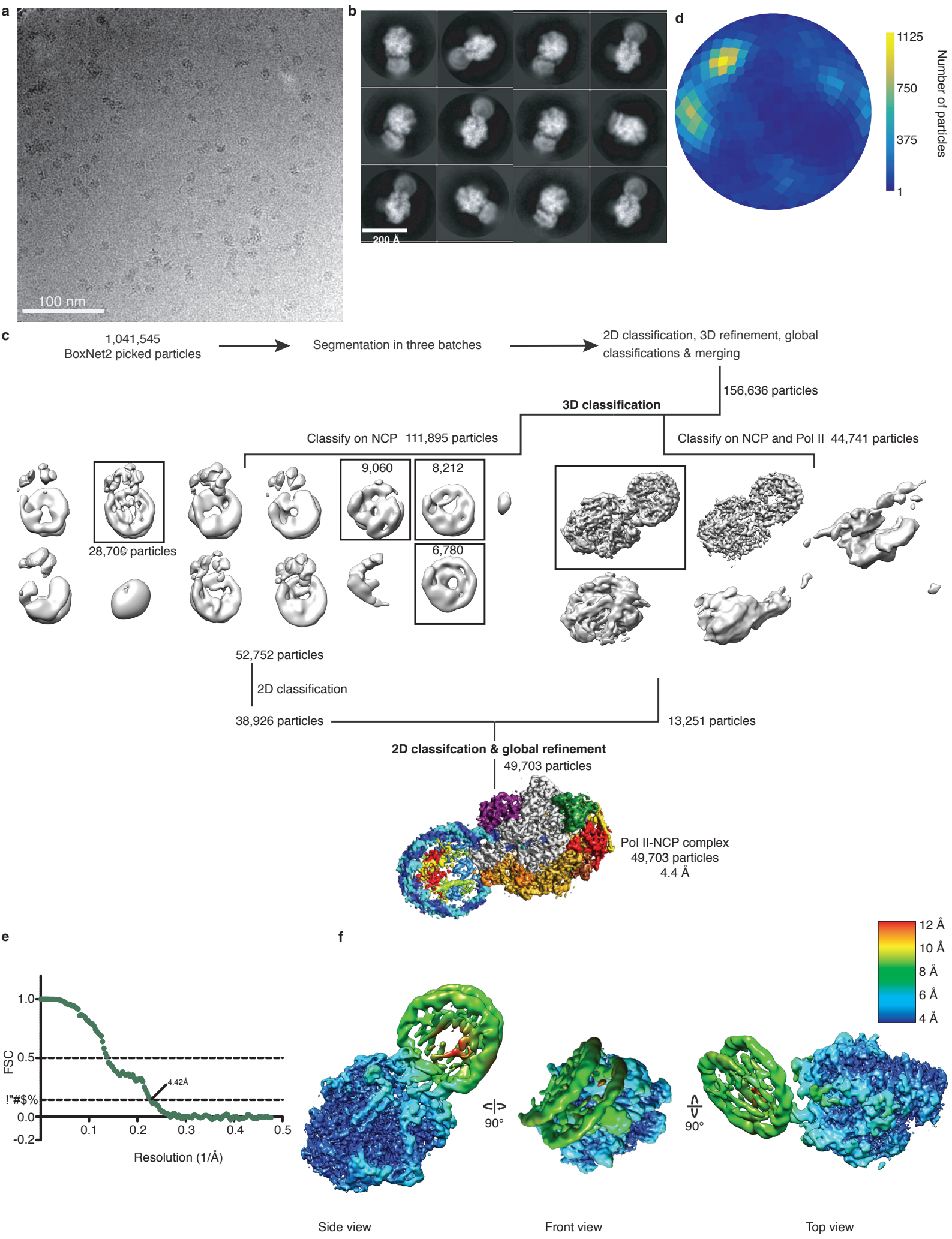

Extended Data Figure 2

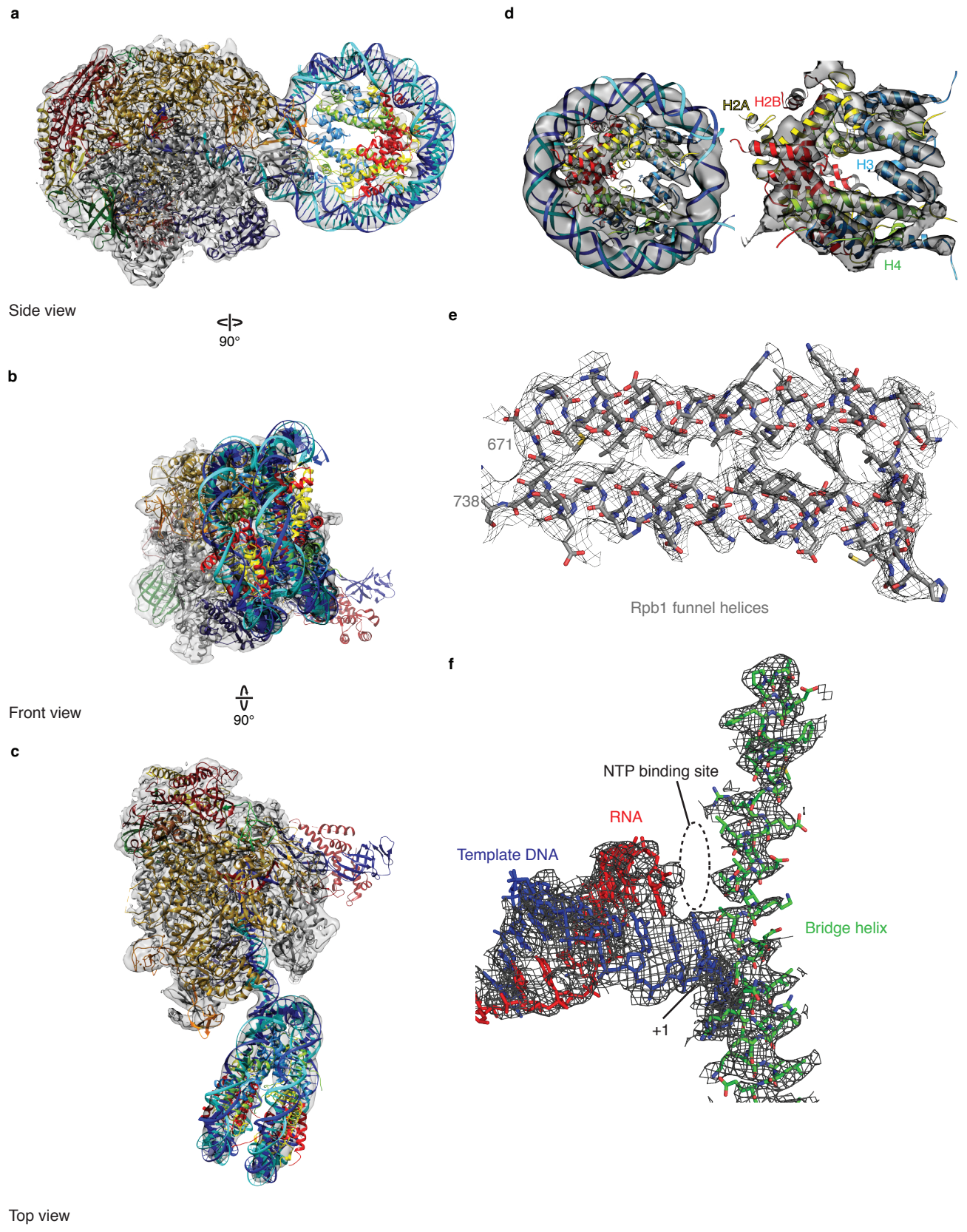

Extended Data Figure 3

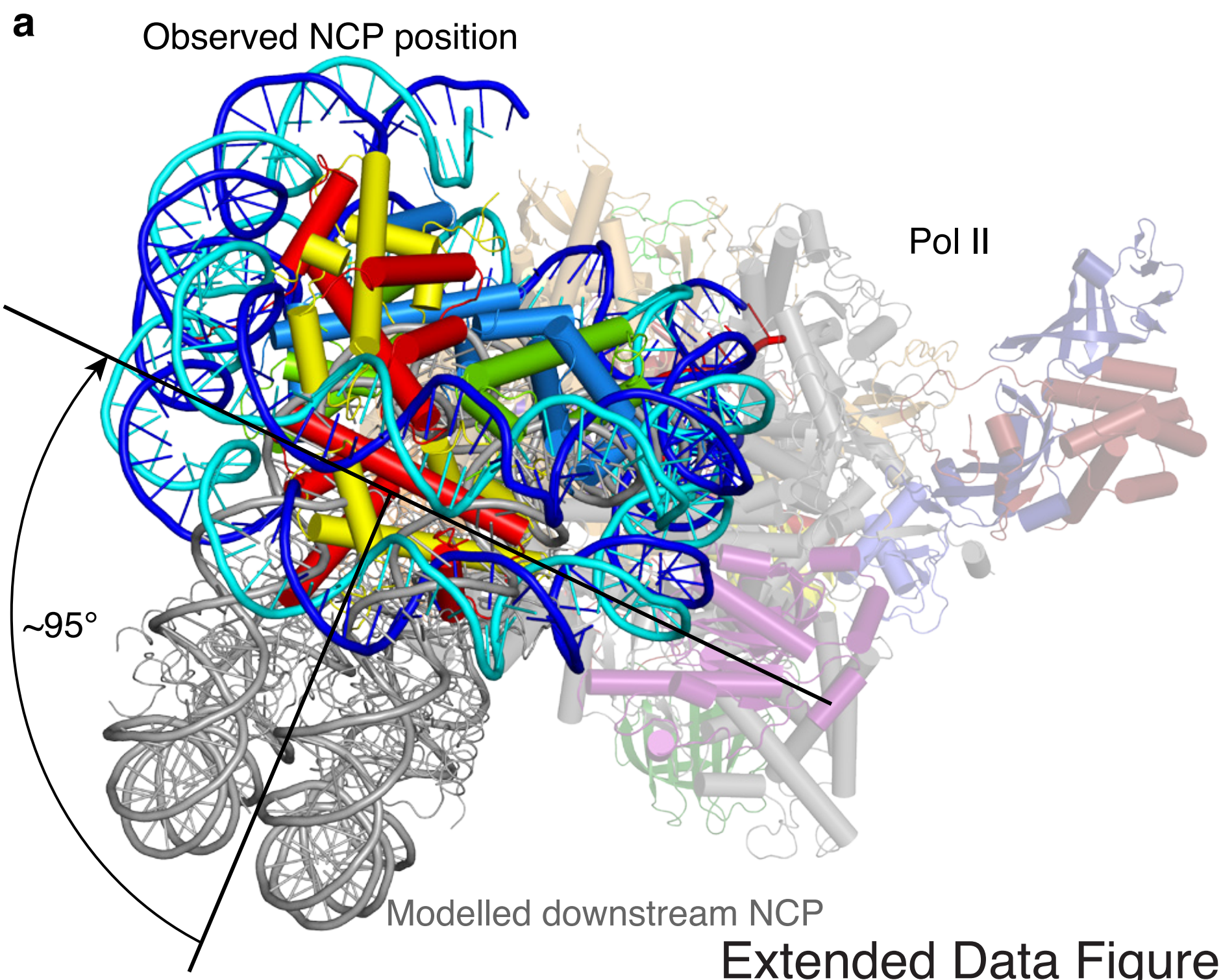

Extended Data Figure 4